ARTICLES

Ternary Stannides Li*T*Sn$_4$ (*T* = Ru, Rh, Ir)—Chemical Bonding and Physical Properties

Zhiyun Wu,[†,‡] Hellmut Eckert,*[,‡] Jürgen Senker,[§] Dirk Johrendt,[||] Gunter Kotzyba,[§] Bernd D. Mosel,[‡] Henning Trill,[‡] Rolf-Dieter Hoffmann,[†] and Rainer Pöttgen*[,†]

Institut für Anorganische und Analytische Chemie and Sonderforschungsbereich 458, Westfälische Wilhelms-Universität Münster, Wilhelm-Klemm-Straβe 8, 48149 Münster, Germany, Institut für Physikalische Chemie and Sonderforschungsbereich 458, Westfälische Wilhelms-Universität Münster, Schlossplatz 4/7, 48149 Münster, Germany, Department Chemie, Ludwig-Maximilians-Universität München, Butenandtstraβe 5-13 (Haus D), 81377 München, Germany, and Institut für Anorganische Chemie und Strukturchemie, Lehrstuhl II, Heinrich-Heine-Universität Düsseldorf, Universitätsstrasse 1, D-40225, Düsseldorf, Germany

Received: September 13, 2002

Pure samples of the ternary stannides Li*T*Sn$_4$ (*T* = Ru, Rh, Ir) have been synthesized from the elements in sealed tantalum tubes. They crystallize with an ordered version of the PdGa$_5$ type. Li*T*Sn$_4$ (*T* = Ru, Rh, Ir) are all metallic conductors and Pauli paramagnets. Spectroscopic measurements indicate significant differences in the chemical bonding properties: As revealed by both ^{119}Sn Mössbauer spectroscopy and solid-state NMR data, the local electron distribution at the tin site is more anisotropic in LiRuSn$_4$ compared to the other two materials. In addition, ^{7}Li Knight shift and spin-lattice relaxation times indicate that LiRuSn$_4$ has a much higher electron density at the lithium atom arising from conduction electrons at the Fermi level. These findings are in good agreement with the results of DFT band structure calculations.

1. Introduction

A new family of intermetallic lithium transition metal stannides of compositions Li*T*Sn$_4$ (*T* = Ru, Rh, Ir), LiPd$_2$Sn$_6$, and LiCoSn$_6$ has recently been reported.[1−3] The common structural motif is the square antiprismatic coordination of the transition metal (*T*) atoms in all of these structures. The [*T*Sn$_8$] square antiprisms are condensed via common edges forming two-dimensional layers of composition [*T*Sn$_4$] which resemble the CuAl$_2$ structure. Stacking of these [*T*Sn$_4$] layers leaves square prismatic voids which are filled by lithium atoms. The structures of Li*T*Sn$_4$, LiPd$_2$Sn$_6$, and LiCoSn$_6$ differ only by the different stacking sequences of the [*T*Sn$_4$] layers.[2]

The pronounced two-dimensional character of the structures of the Li*T*Sn$_4$ (*T* = Ru, Rh, Ir) stannides (Figure 1) readily implies a potential lithium mobility within the *ab* plane. Such intermetallic materials may find application as alloy electrodes for batteries.[4] We have now started a systematic investigation of the physical properties of these stannides mainly with respect to a potential lithium mobility. The magnetic susceptibility, electrical resistivity, ^{119}Sn Mössbauer, and ^{7}Li MAS solid-state NMR spectroscopic data are reported herein. Furthermore we elucidated chemical bonding in more detail in order to establish first structure−property relations.

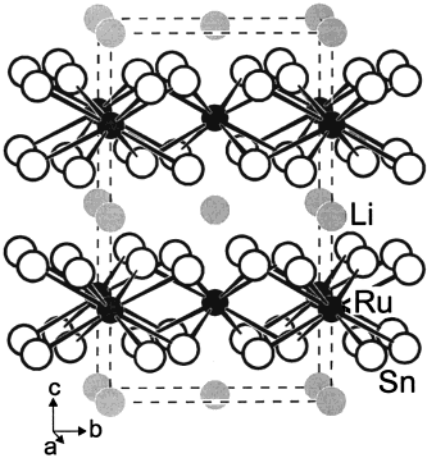

Figure 1. Crystal structure of LiRuSn$_4$. The two-dimensional [RuSn$_4$] network is emphasized.

2. Experimental Section

2.1. Sample Preparation. Starting materials for the preparation of the Li*T*Sn$_4$ (*T* = Ru, Rh, Ir) stannides were lithium rods (Merck), powders of ruthenium, rhodium, and iridium (Degussa-Hüls, 200 mesh), and a tin bar (Heraeus) all with stated purities better than 99.9 %. The elements were mixed in the ideal atomic ratio and sealed in tantalum tubes under an argon pressure of about 600 mbar.[5] The tantalum tubes were sealed in silica

* Author to whom correspondence should be addressed at Institut für Anorganische und Analytische Chemie, Westfälische Wilhelms-Universität Münster, Wilhelm-Klemm-Straβe 8, 48149 Münster, Germany. Tel.: +49-251-83-36001. Fax: +49-251-83-36002. E-mail: pottgen@uni-muenster.de.

† Institut für Anorganische und Analytische Chemie and Sonderforschungsbereich 458, Westfälische Wilhelms-Universität Münster.

‡ Institut für Physikalische Chemie and Sonderforschungsbereich 458, Westfälische Wilhelms-Universität Münster.

§ Ludwig-Maximilians-Universität München.

|| Heinrich-Heine-Universität Düsseldorf.

10.1021/jp0220635 CCC: $25.00 © 2003 American Chemical Society
Published on Web 02/07/2003

ampoules, rapidly heated at 1220 K, slowly cooled at 870 K within 3 hours, held at that temperature for one week, and finally quenched by radiative heat loss. The polycrystalline samples were obtained in amounts of 1−2 g. They are stable in moist air. For more details concerning the sample preparation we refer to our previous work.[3]

The purity of the Li*T*Sn$_4$ samples was checked through Guinier powder patterns using Cu Kα_1 radiation and α-quartz (a = 491.30, c = 540.46 pm) as an internal standard. The experimental patterns were compared with calculated ones[6] using the positional parameters of the refined structures.[3] The lithium content was checked through ICP-AES analyses as described earlier.[3]

2.2. Physical Property Measurements. The magnetic susceptibilities of Li*T*Sn$_4$ (T = Ru, Rh, Ir) were determined with a MPMS *XL* SQUID magnetometer (Quantum Design, Inc.) in the temperature range 2 K ≤ T ≤ 300 K with magnetic flux densities up to 5 T. Resistivity measurements were performed on polycrystalline pieces (edges up to 2 mm) of LiRhSn$_4$ and LiIrSn$_4$ using a four-probe technique. A constant current (Keithley Source Meter 2400) was applied to the samples and the resulting voltage was measured with a Keithley nanovoltmeter 2182. The four silver contacts were glued to the samples with a well conducting silver adhesive. The samples were fixed on a closed-cycle cooling system (Cryodyne 22 CP, CTI-Cyrogenics) using a low-temperature adhesive (Cryophysics, 7031 insulating Varnish and Adhesive). The temperature was controlled by a silicon diode (Lake Shore, model 330) between 8 and 320 K with an accuracy better than ±0.1 K. In each measurement the temperature was varied up and down in steps of 2 K.

2.3. ^{119}Sn Mössbauer and Solid-State NMR Spectroscopy. A Ca^{119m}SnO$_3$ source was available for the ^{119}Sn Mössbauer spectroscopy investigations. The samples were placed within thin-walled PVC containers at a thickness between 10 and 15 mg Sn/cm^2. A palladium foil of 0.05 mm thickness was used to reduce the tin K X-rays concurrently emitted by this source. The measurements were conducted in the usual transmission geometry at various temperatures.

All the ^{7}Li and ^{119}Sn solid-state NMR measurements were carried out at 155.5 and 149.8 MHz, respectively, using a Bruker DSX 400 spectrometer equipped with a 4 mm MAS-NMR probe. Typical spinning speeds ranged from 8 to 15 kHz. For ^{119}Sn NMR, a relaxation delay of 0.5 s was used, for ^{7}Li NMR the delays were 4, 10, and 20 s for the compounds LiRuSn$_4$, LiRhSn$_4$, and LiIrSn$_4$, respectively. To minimize undesirable effects of probe detuning and sample heating of these highly metallic samples, the finely ground powders were mixed with silica in a 1:2 mass ratio. Variable temperature ^{7}Li NMR lineshapes and spin-lattice relaxation times (measured by the saturation recovery technique) were obtained between 200 and 450 K using a Bruker BVT 3000 digital temperature controller.

2.4. Electronic Structure Calculations. The chemical bonding analysis was carried out by self-consistent DFT-LDA band structure calculations for LiRuSn$_4$ and LiRhSn$_4$ using the LMTO-method in its scalar-relativistic version (program TB-LMTO-ASA).[7] Detailed descriptions are given elsewhere.[8, 9] Reciprocal space integrations were performed with the tetrahedron method.[10] The basis sets consisted of 2*s*/2*p*/3*d* for Li, 5*s*/5*p*/4*d* for Ru and Rh, and 5*s*/5*p*/5*d*/4*f* for Sn. The 2*p*/3*d* orbitals of Li and 5*d*/4*f* of Sn were treated by the downfolding technique.[11] In order to achieve space filling within the atomic sphere approximation, interstitial spheres are introduced to avoid too large overlap of the atom-centred spheres. The COHP (Crystal Orbital Hamilton Population) method was used for the bond analysis.[12] COHP gives the energy contributions of all electronic states for a selected bond. The values are negative for bonding and positive for antibonding interactions. With respect to the well-known COOP diagrams, we plot −COHP(E) to get positive values for bonding states.

Theoretical values of the electrical field gradients were obtained from full-potential linearized augmented plane wave (LAPW) calculations within the generalized gradient approximation,[13] as implemented in the WIEN2k code.[14] The muffin-tin sphere radii R_i = 2.0, 2.1, and 2.1 a.u were used for Li, (Rh, Ru, Ir) and Sn, respectively. The expansions of the wave functions included about 1780 LAPWs up to RK_{max} = 8.0 and about 170 local orbitals for semi-core states within the same energy window. We used a 10 × 10 × 10 mesh which represents 99 k points in the irreducible wedge of the Brillouin-zone.

3. Results and Discussion

3.1. Crystal Chemistry and Electronic Structure. The crystal chemistry of the stannides Li*T*Sn$_4$ (T = Ru, Rh, Ir) has been described in detail in reference 3. We give only a short summary here and discuss the structural features relevant for the physical properties and the spectroscopic data. The Li*T*Sn$_4$ stannides (space group *I*4/*mcm*) crystallize with an ordered variant of the PdGa$_5$ type. The transition metal atoms have a square-antiprismatic tin coordination. These square anti-prisms are condensed via common faces forming two-dimensional [*T*Sn$_4$] polyanions which are separated by the lithium atoms (Figure 1). Each lithium atom has a near-neighbor environment of eight tin atoms in the form of slightly compressed cubes at Li−Sn distances of 292 pm (LiRuSn$_4$) and 291 pm (LiRhSn$_4$ and LiIrSn$_4$). The c/a ratios of the LiSn$_8$ cubes are 0.869, 0.888, and 0.891 for the Ru, Rh, and Ir compound, respectively. The Ru−Sn, Rh−Sn, and Ir−Sn distances of 279, 280, and 280 pm, respectively, within the two-dimensional [*T*Sn$_4$] polyanions are slightly larger than the sum of the covalent radii[15] of 265 pm (Ru + Sn /Rh + Sn) and 266 pm (Ir + Sn). The various Sn−Sn distances in the Li*T*Sn$_4$ stannides range from 294 to 352 pm, similar to those in the β-tin structure (4 × 302 and 2 × 318 pm).[16] Based on these distances we expect also a significant degree of Sn−Sn bonding besides strong *T*−Sn bonding. Comparing the nearest neighbor coordinations, the structures of LiRuSn$_4$ and LiRhSn$_4$ are almost similar. We have therefore performed electronic structure calculations in order to elucidate the differences in chemical bonding.

The results of DFT-LDA band structure calculations show almost identical electronic properties for LiRuSn$_4$ and LiRhSn$_4$, as expected from the similar structures. The main differences from the electronic viewpoint emerge from the one additional electron per formula unit for the rhodium compound, which leads to higher band filling. Figure 2 shows the electronic density of states (DOS) of Li*T*Sn$_4$ with T = Ru and Rh together with the projections of states from lithium, tin, and transition metal. The different Fermi levels for T = Ru and T = Rh are indicated. No energy gaps discern at E_F, where the DOS are roughly composed of 65% tin, 30% transition metal, and 5% Li states. Although the composition of the DOS at the Fermi energy are almost the same for both stannides, we find an almost doubled density of states value at E_F for the ruthenium compound (Figure 2). We can therefore expect perceptible differences in spectroscopic properties, which are susceptible to the conduction electron density. LiRuSn$_4$ and LiRhSn$_4$ are clearly expected to be metallic, which is confirmed by resistivity measurements for

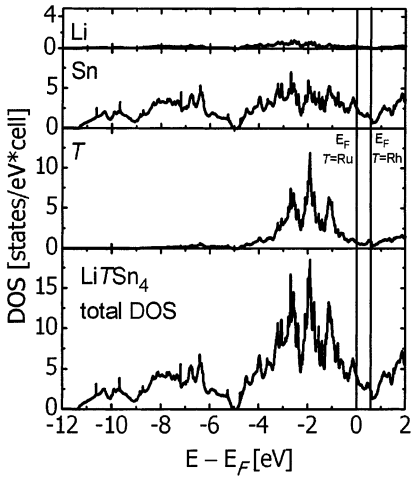

Figure 2. Electronic density of states of LiTSn$_4$ with T = Ru and Rh. The different Fermi levels for the ruthenium and rhodium compound are indicated as vertical lines.

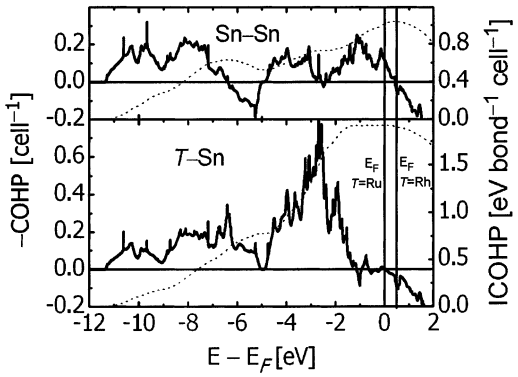

Figure 3. Crystal orbital Hamiltonian population (COHP) diagrams of the T−Sn and Sn−Sn bonds in LiRuSn$_4$ and LiRhSn$_4$. Dotted lines represent the COHP integrations.

the rhodium and iridium stannide. The DOS-projection of the tin states shows a wide energy range of the tin crystal orbitals. Almost no energy separation of Sn 5*s* and 5*p* levels occurs, and especially the broadening of the 5*s* states from −5 to −12 eV is remarkable. Thus, the tin 5*s* orbitals are strongly involved in Sn−Sn and T−Sn bonding and show no lone pair character. Although the lithium contribution to the DOS is small (Figure 2), we find some occupation of Li states. From this we infer a positively polarized $Li^{\delta+}$, which transfers charge to the $[TSn_4]^{\delta-}$ polyanions, but lithium is not completely ionized.

As seen from the COHP diagrams in Figure 3, the strongest bonds are the T−Sn interactions. The Ru−Sn bonding states are completely filled in LiRuSn$_4$, whereas some Rh−Sn antibonding states get occupied in LiRhSn$_4$. However, this small amount does not weaken the Rh−Sn bond significantly. For the Sn−Sn bonds, whose bonding energy (ICOHP) is roughly 50% of a T−Sn bond, we find the opposite effect. A small amount of Sn−Sn bonding states are empty in LiRuSn$_4$, but filled in LiRhSn$_4$ through the additional electron of rhodium. Thus, the higher valence electron count in going from LiRuSn$_4$ to LiRhSn$_4$ leads to weaker T−Sn and stronger Sn−Sn bonding.

The DOS diagrams obtained from the LAPW calculations of LiRuSn$_4$ and LiRhSn$_4$ are nearly identical with the presented LMTO results and reproduce the above-mentioned trend of the DOS at E_F. The calculated electrical field gradient (EFG) at the tin site in LiRuSn$_4$ is much larger than in LiRhSn$_4$ and LiIrSn$_4$. The EFG ratio for the Ru, Rh, and Ir compound is 1:0.62:0.58. This is in excellent agreement with the experimental

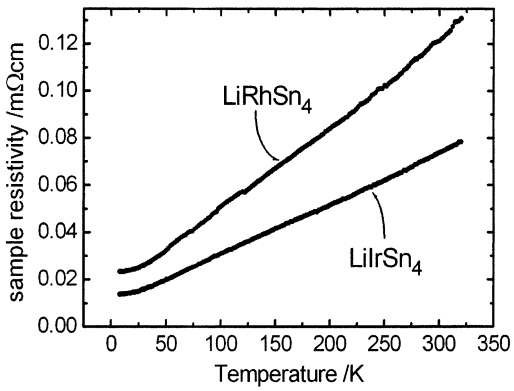

Figure 4. Temperature dependence of the specific resistivity of LiRhSn$_4$ and LiIrSn$_4$.

TABLE 1: Fitting parameters of ^{119}Sn Mössbauer Measurements in LiTSn$_4$ (T = Ru, Rh, Ir) (Numbers in parentheses represent the statistical errors in the last digit. Γ: experimental linewidth; δ: isomer shifts; ΔE_Q: electric quadrupole interaction.)

T (K)	δ (mm/s)	ΔE_Q (mm/s)	Γ (mm/s)
	LiRuSn$_4$		
298	2.158(3)	1.02(6)	0.81(3)
250	2.163(2)	1.01(5)	0.84(3)
200	2.178(6)	1.02(8)	0.87(6)
150	2.190(5)	1.00(5)	0.87(6)
100	2.199(5)	1.01(6)	0.89(5)
49	2.223(5)	1.01(4)	0.91(4)
4.2	2.214(4)	1.03(8)	0.92(4)
	LiRhSn$_4$		
298	2.21(2)	0.65(5)	0.82(6)
249	2.22(1)	0.64(4)	0.81(5)
200	2.24(1)	0.64(4)	0.89(6)
150	2.25(1)	0.64(4)	0.91(5)
100	2.26(1)	0.65(5)	0.92(4)
50	2.27(1)	0.65(5)	1.18(7)
5	2.27(2)	0.62(6)	1.03(9)
	LiIrSn$_4$		
298	2.121(5)	0.59(2)	0.88(4)
232	2.13(1)	0.59(4)	0.90(6)
172	2.150(7)	0.59(2)	0.91(4)
110	2.16(1)	0.61(4)	0.93(6)
52	2.169(5)	0.62(1)	0.96(2)
4.2	2.174(5)	0.62(1)	0.95(2)

values obtained from Mössbauer spectroscopy, yielding 1:0.64:0.58 (Table 1). However, the calculated absolute values of the EFG (LiRuSn$_4$: 13.3×10^{21}, LiRhSn$_4$: 8.3×10^{21}, LiIrSn$_4$: 7.8×10^{21} V m^{-2}) deviate from the experimental values by about 40%.

3.2. Electrical and Magnetic Properties. The specific resistivity data of LiRhSn$_4$ and LiIrSn$_4$ are displayed in Figure 4. With decreasing temperature we observe decreasing specific resistivities, as is typical for metallic conductors. This behavior is in excellent agreement with the non-vanishing DOS observed in the electronic structure calculations. The resistivity ratios ρ(4.2 K)/ρ(320 K) are 0.17 for LiRhSn$_4$ and 0.16 for LiIrSn$_4$. The room temperature specific resistivity values are 130 $\mu\Omega$cm (LiRhSn$_4$) and 80 $\mu\Omega$cm (LiIrSn$_4$).

The temperature dependence of the magnetic susceptibilities of LiTSn$_4$ (T = Ru, Rh, Ir) is shown in Figure 5. Over the whole temperature range the susceptibilities are negative. At first sight, one might think the stannides are diamagnets. This, however, is in contrast to the metallic behavior observed from the resistivity measurements. According to the poor metallic conductivity and the small density of states at the Fermi level, the Pauli contribution of the conduction electrons is only small.

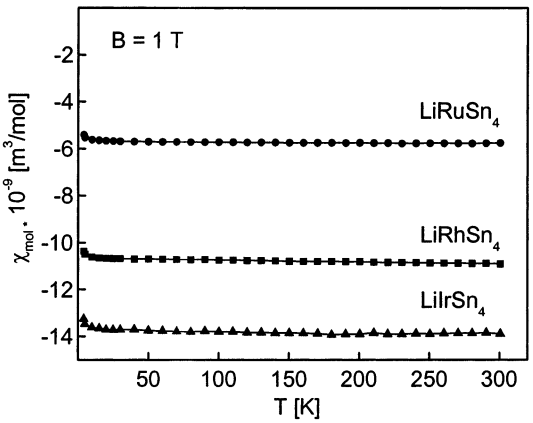

Figure 5. Temperature dependence of the magnetic susceptibility of Li*T*Sn$_4$ (*T* = Ru, Rh, Ir) measured at a magnetic flux density of 1 T.

The large core diamagnetism (mainly contributed from the tin atoms) has a larger absolute value than the Pauli contribution, resulting in negative total susceptibilities over the whole temperature range. At low temperatures, we observe only very small upturns of the susceptibility data indicating only trace amounts of paramagnetic impurities, i.e., the samples investigated are magnetically very pure.

3.3. ^{119}Sn Mössbauer and Solid-State NMR Spectroscopy. Temperature-dependent ^{119}Sn Mössbauer spectra of Li*T*Sn$_4$ (*T* = Ru, Rh, Ir) are shown in Figure 6 together with transmission integral fits. The fitting parameters are listed in Table 1. While the isomer shifts fall into the usual range observed in intermetallic stannides, significant differences are observed in the magnitude of the nuclear electric quadrupolar splittings. The data appear to be correlated with the valence electron count (VEC) of the transition metal ion. LiRuSn$_4$ (VEC = 8) shows a rather large quadrupolar splitting of ~1.00 mm/s over the entire temperature range investigated. In contrast, LiRhSn$_4$ and LiIrSn$_4$ (VEC = 9) show significantly smaller quadrupole splittings of 0.65 and 0.59 mm/s, respectively. These results indicate that the electron distribution at the tin nuclei is more asymmetric in LiRuSn$_4$ as compared to the other two compounds. The difference agrees with the change in *T*−Sn and Sn−Sn bonding reflected in the band structure calculations, which are also able to reproduce the experimental trend among the three compounds (see above). Other experimental indications of significant differences in tin bonding come from the ^{119}Sn NMR spectra displayed in Figure 7. While LiRuSn$_4$ shows a well-resolved MAS-NMR sideband pattern revealing a sizeable chemical shift anisotropy, the corresponding spectra of the Rh and Ir compounds are rather ill-defined, signifying a smaller anisotropy and more disorder. The isotropic chemical shifts determined from the center of gravity are 4172 ppm, 3970 ppm, and 4680 ppm for the Ru, Rh, and Ir compounds, respectively. For both LiRhSn$_4$ and LiIrSn$_4$, the rather large MAS-NMR linewidths reflect a wide distribution of isotropic chemical shifts. The detailed structural or electronic origin for this distribution is unknown at the present time. To provide a basis for a future interpretation of such effects, we are currently developing a ^{119}Sn chemical shift data base on intermetallic compounds.

Figure 8 summarizes the ^{7}Li MAS NMR spectra of the three compounds investigated. All three compounds show a single well-resolved centerband consistent with the existence of a single lithium site. In addition, each spectrum contains a spinning sideband manifold caused by the effect of slow MAS on the anisotropically broadened $|\pm 1/2> \leftrightarrow |\pm 3/2>$ satellite transitions, which are caused by first-order quadrupolar perturbations. The ^{7}Li nuclear electric quadrupolar coupling constants extracted at 200 K from the intensity profiles via simulation are 148, 116, and 140 kHz for LiRuSn$_4$, LiRhSn$_4$, and LiIrSn$_4$, respectively. The axial symmetry of the electric field gradient deduced from these simulations is consistent with the 4/*m* point symmetry of the Li site known from the crystal structure. For all three compounds, the electric field gradients decrease only slightly (~5%) over the temperature range 200 K ≤ *T* ≤ 450 K. This finding documents the absence of long-range ionic diffusion. Since the Li site is fully occupied, ionic diffusion in these compounds must take place involving interstitial sites. The electric field gradient tensors of the regular and the interstitial sites are expected to differ markedly and thus diffusion should lead to a marked reduction of the nuclear electric quadrupolar interaction. This is, however, not observed in our experiments.

To probe for more localized motional processes (rattling of the Li atom on its site), we have also measured the static ^{7}Li NMR spectra as a function of temperature. Typical data are summarized in Figure 9. In all cases, the static linewidths as measured at 200 K exceed the purely dipolar values calculated from the van-Vleck equation. Complementary measurements conducted at 77.7 MHz on a 4.65 T magnet reveal that the

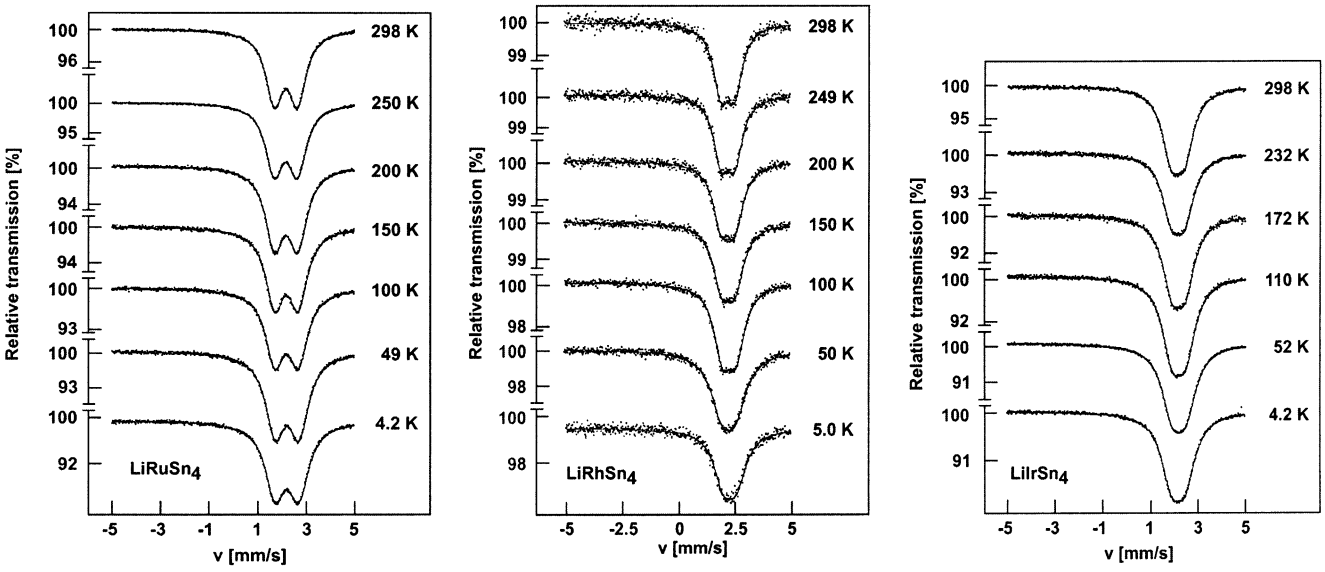

Figure 6. Experimental and simulated ^{119}Sn Mössbauer spectra of Li*T*Sn$_4$ (*T* = Ru, Rh, Ir) at various temperatures.

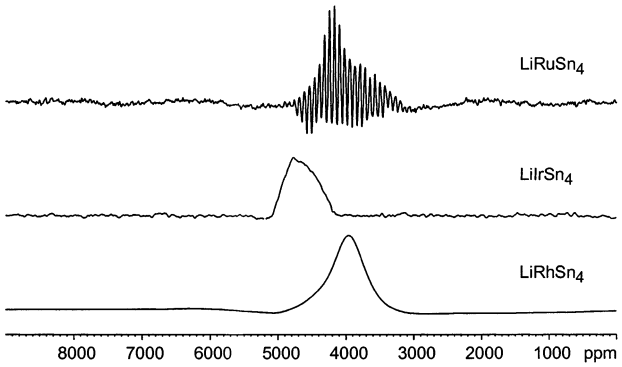

Figure 7. ^{119}Sn MAS-NMR spectra of LiRuSn$_4$, LiIrSn$_4$, and LiRhSn$_4$. For further details, see text.

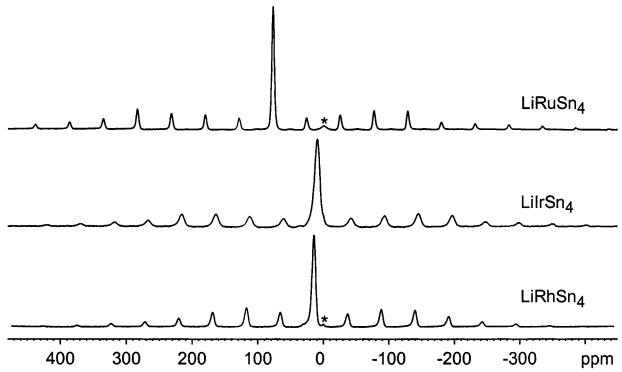

Figure 8. ^{7}Li MAS-NMR spectra of LiRuSn$_4$, LiIrSn$_4$, and LiRhSn$_4$. Oxidic impurities are marked by asterisks. The intensities of these resonances are reduced owing to the relatively short relaxation delays used. In each spectrum the dominant peak is the MAS centerband of the central transition, the other peaks are spinning sidebands arising from the quadrupolar satellite transitions.

linewidth contains a linearly field-dependent contribution arising from anisotropic shielding. This contribution is most clearly evident in the rigid lattice spectrum of LiRuSn$_4$, producing a pronounced lineshape asymmetry of the central transition. As a result, the satellite transition spinning sideband manifold arises from the combined effect of chemical shift anisotropy (csa) and nuclear electric quadrupolar coupling. A corresponding simulation of the spinning sideband pattern, using the SIMPSON program, was carried out for LiRuSn$_4$, indicating an axially symmetric shielding tensor with an anisotropy of 32 ppm. Most significantly, the ^{7}Li shielding and quadrupolar interaction tensors are coincident, (the angle between both principal axes is zero degrees) consistent with the ^{7}Li local site symmetry. Inspection of the static spectra in the rigid lattice limit suggests that the csa is significantly larger for the ruthenium compound in comparison to the other materials. Furthermore, Figure 9 illustrates a moderate reduction in linewidth and shift anisotropy at elevated temperatures, suggesting an increase of the thermal displacement of the lithium ions with increasing temperature. Again, these data reflect the absence of long-range diffusion within the temperature range investigated.

While the ^{7}Li electric field gradients and the ion motional characteristics are rather similar for LiRuSn$_4$, LiIrSn$_4$, and LiRhSn$_4$, marked differences are observed for the MAS centerband positions, revealing large differences in the chemical bonding character of the Li ions. The large shift observed in LiRuSn$_4$ (76.8 ppm at 300 K) can be explained in terms of a scalar magnetic coupling ("Fermi contact interaction") between the ^{7}Li nuclei and unpaired *s*-electron density at the Fermi level producing a "Knight shift",

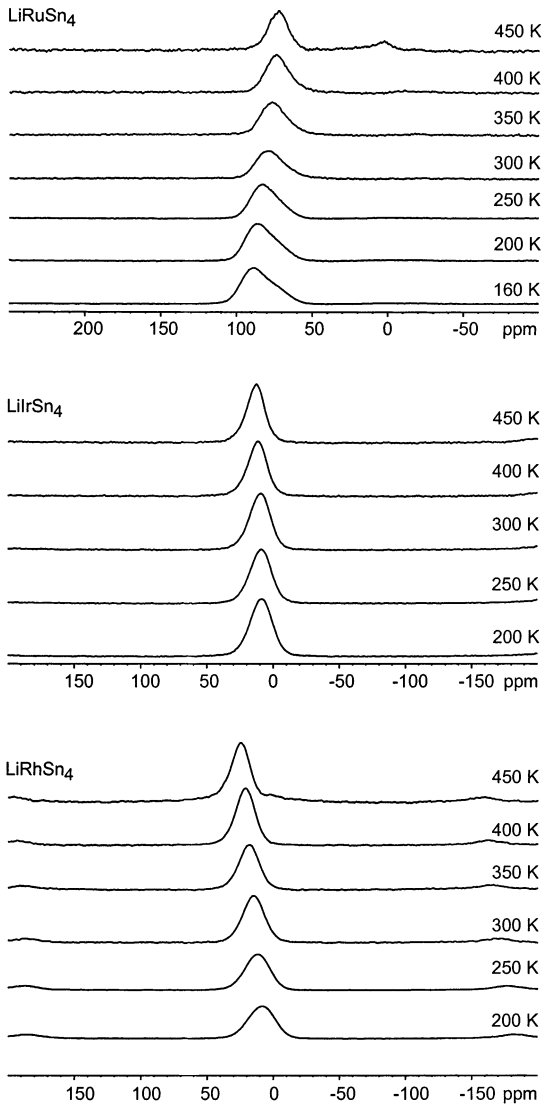

Figure 9. Variable temperature static NMR spectra of LiRuSn$_4$, LiIrSn$_4$, and LiRhSn$_4$. Resonances near 0 ppm arise from oxidic impurities.

$$\delta = \frac{8\pi}{3} |\phi(0)|_{E_F}{}^2 \chi_e^s$$

where χ_e^s is the electron spin susceptibility and $|\phi(0)|_{E_F}{}^2$ is the density of conduction electrons at the Fermi level probed at the nuclear sites. In contrast, the resonance shifts measured for the Rh and Ir compounds (9.5 and 14.6 ppm) are much smaller, indicating lower *s*-electron densities consistent with more ionic/covalent rather than metallic lithium bonding in these two materials. Furthermore, all three compounds show significant chemical shift temperature coefficients (see Table 2), indicating that the *s*-electron densities increase significantly with temperature in LiRhSn$_4$ and LiIrSn$_4$, whereas in LiRuSn$_4$ just the opposite effect is observed.

Further insights into the bonding properties and dynamics of the lithium ions are potentially available from spin-lattice relaxation time (T_1) measurements. In general, the interpretation of T_1 data in mixed conductors is rather complex, since the ^{7}Li nuclear spins can be relaxed by a variety of physical mechanisms, including magnetic dipole and electric field gradient fluctuations caused by ion dynamics occurring at frequencies in the MHz region. For the present materials, this relaxation mechanism is likely to have only minor importance as the

TABLE 2: Temperature-Dependent ^{7}Li NMR Parameters of Li*T*Sn$_4$ (*T* = Ru, Rh, Ir)

	$LiRuSn_4$		$LiRhSn_4$		$LiIrSn_4$	
T (K)	δ_{iso}/ ppm[a]	T_1^{-1} (s^{-1})	δ_{iso}/ ppm[a]	T_1^{-1} (s^{-1})	δ_{iso}/ ppm[a]	T_1^{-1} (s^{-1})
450	71.8	1.63	25.2	0.42	13.7	0.24
400	72.1	1.60	21.8	0.36	12.3	0.18
350	74.6	1.51	18.7	0.28	11.2	0.13
300	76.8	1.27	15.3	0.20	10.0	0.10
250	80.6	0.96	12.3	0.15	9.6	0.07
200	82.8	0.84	10.5	0.10	9.2	0.05

[a] Center of gravity obtained from the static spectra.

temperature-dependent lineshape data indicate that the ion dynamics in these compounds are rather slow and restricted. Rather, we attribute the relaxation predominantly to the Fermi contact mechanism, i.e., to nuclear spin fluctuations of unpaired electrons near the Fermi-level, which have a finite probability $|\phi(0)|^2_{E_F}$ at the nuclear sites. As the number of these electrons is proportional to k_BT, the spin-lattice relaxation rate of nuclei in a metal increases linearly with increasing temperature:

$$\frac{1}{T_1} = a|\phi(0)|^2_{E_F}\rho^2(E_F)k_BT$$

where $\rho(E_F)$ is the density of states at the Fermi-level, k_BT is the thermal energy, and a is a constant. Consistent with this interpretation, Table 2 reveals that $1/T_1$ increases approximately linearly with temperature in all three compounds. Furthermore, the spin-lattice relaxation rate is about one order of magnitude larger in $LiRuSn_4$ than in the other two compounds, suggesting again, in agreement with the Knight shift data, that $|\phi(0)|^2_{E_F}$ is significantly larger in $LiRuSn_4$ than in the corresponding Rh and Ir compounds. This finding is correlated with the band structure calculation results inasmuch as the latter reveal that the Ru compound has almost twice the density of states at E_F compared to the Rh compound. Small differences in the specific Li contributions to the DOS are difficult to extract from calculations. The NMR technique appears to be the more sensitive local probe providing a direct experimental approach to this effect.

Acknowledgment. We thank the Degussa-Hüls AG for a generous gift of noble metals. This work was financially supported by the Fonds der Chemischen Industrie and by the Deutsche Forschungsgemeinschaft through SFB 458 *Ionenbewegung in Materialien mit ungeordneten Strukturen*.

References and Notes

(1) Wu, Zh.; Hoffmann, R.-D.; Pöttgen, R. *Z. Kristallogr*. **2002,** *Suppl. 19*, 126.

(2) Pöttgen, R.; Wu, Zh.; Hoffmann, R.-D.; Kotzyba, G.; Trill, H.; Senker, J.; Johrendt, D.; Mosel, B. D.; Eckert, H. *Heteroatom Chem*., 2002.

(3) Wu, Zh.; Hoffmann, R.-D.; Pöttgen, R. *Z. Anorg. Allg. Chem*. **2002,** *628*, 1484.

(4) Huggins, R. A. Lithium Alloy Electrodes. In *Handbook of Battery Materials*; Besenhard, J. O., Ed.; Wiley-VCH: Weinheim, 1999.

(5) Pöttgen, R.; Gulden, Th.; Simon, A. *GIT Labor-Fachzeitschrift* **1999,** *43*, 133.

(6) Yvon, K.; Jeitschko, W.; Parthé, E. *J. Appl. Crystallogr*. **1977,** *10*, 73.

(7) Andersen, O. K.; Jepsen, O. *Tight-Binding LMTO Vers. 47*; Max-Planck-Institut für Festkörperforschung: Stuttgart, 1994.

(8) Jepsen, O.; Snob, M.; Andersen, O. K. *Linearized Band Structure Methods and its Applications*; Springer Lecture Notes; Springer: Berlin 1987.

(9) Skriver, H. L. *The LMTO Method*; Springer: Berlin, 1984.

(10) Andersen, O. K.; Jepsen, O. *Solid State Commun*. **1971,** *9*, 1763.

(11) Lambrecht, W. R. L.; Andersen, O. K. *Phys. Rev. B* **1986,** *34*, 2439.

(12) Dronskowski, R.; Blöchl, P. *J. Phys. Chem*. **1993,** *97*, 8617.

(13) Perdew, J. P.; Chevary, J. A.; Vosko, S. H.; Jackson, A.; Pederson, M. R.; Singh, D. J.; Fiolhais, C. *Phys. Rev. B* **1992**, *46*, 6671.

(14) Blaha, P.; Schwarz, K.; Luitz, J. *WIEN2k, An Augmented Plane Wave Plus Local Orbitals Program*; Vienna University of Technology, 2001.

(15) Emsley, J. *The Elements*; Clarendon Press: Oxford, 1989.

(16) Donohue, J. *The Structures of the Elements*; Wiley: New York, 1974.